Journal of Quantitative Spectroscopy & Radiative Transfer 278 (2022) 108018

Contents lists available at ScienceDirect

Journal of Quantitative Spectroscopy & Radiative Transfer

journal homepage: www.elsevier.com/locate/jqsrt

Dependent scattering effects in aggregates with touching or overlapping non-absorbing spherical particles

Tiphaine Galy*, Laurent Pilon

Mechanical and Aerospace Engineering Department Henry Samueli School of Engineering and Applied Science, University of California, Engineering IV 420 Westwood Plaza, Los Angeles, CA 90095-1597, USA

ARTICLE INFO

Article history:
Received 25 February 2021
Revised 24 November 2021
Accepted 25 November 2021
Available online 26 November 2021

Keywords:
Electromagnetic scattering
Light scattering
Dependent scattering
Equivalent sphere approximations
Aerogels atmospheric dust

ABSTRACT

This study evaluates the effect of dependent scattering and particle overlapping on the integral radiation characteristics of fractal aggregates of monodisperse and non-absorbing spherical particles for a wide range of particle and aggregate sizes. It also aims to identify a scattering approximation capable of rapidly predicting these radiation characteristics. The scattering cross-section and asymmetry factor of fractal aggregates with touching or overlapping spherical particles were computed using the *T*-matrix method or the discrete-dipole approximation, respectively. The simulated aggregates were composed of up to 30,000 spherical particles with size parameter x_s varying from 0.03 to 5 for an aggregate size parameter χ_s of up to 23. The results established that dependent effects (i) were more significant in the scattering cross-section and asymmetry factor than in the absorption cross-sections and (ii) increased with decreasing particle size parameter x_s. In addition, overlapping of particles was found to have a negligible effect on the integral radiation characteristics of the aggregates. Finally, the scattering cross section and asymmetry factor of any aggregates consisting of particles such that $x_s \leq 1$ could be predicted by the so-called equivalent effective property (EEP) approximation treating the aggregates as equivalent homogeneous spheres with the same diameter and with effective refractive index given by the Maxwell–Garnett effective medium approximation.

1. Introduction

Light scattering by aggregates consisting of spherical particles is of interest to a wide range of applications. For example, atmospheric dusts consist of clusters of agglomerated primary dust particles with size ranging from tenths to hundreds of microns, as illustrated in Fig. 1(a) [1,2]. Scattering of radiation from UV to near IR by such atmospheric aerosols is essential to predict their effect on the Earth climate [3,4]. In addition, oxide particles, such as titania particles [Fig. 1(b)], are used in paints [5] and self-cleaning window coatings [6,7] and range from tens to hundreds of nanometers in diameter [8,9]. The appearance and performance of such paints and coatings depend on light scattering by titania particle aggregates [5–8]. Furthermore, transparent mesoporous silica monoliths, consisting of a highly porous network of overlapping silica nanoparticles with radius $r_s \leq 20$ nm [Figs. 1(c) and 1(d)], have been considered for solar thermal applications [10–12] and for transparent and thermally insulating window solutions [13–15]. The optical transmittance and haziness of mesoporous silica monoliths depend on their scattering characteristics in the visible part of the electromagnetic spectrum [16]. In all these applications, the incident radiation is unpolarized and its transport through the particulate media is governed by the radiative transfer equation (RTE). Then, knowledge of the integral scattering characteristics of the aggregates, namely their absorption and scattering cross-sections and their asymmetry factor, is of prime importance to predict reflectance, transmittance, haze and other performance metrics, as illustrated in Refs. [17–19].

In systems with sufficiently distant particles, the scattering characteristics can be expressed implicitly or explicitly from those of the individual particles [20,21]. This approach assumes that particles scatter independently from one another, and is often referred to as the "independent scattering regime" [21–23]. Then, the scattering cross-section of the particle ensemble is simply given by the sum of the scattering cross-sections of all particles [20]. When the particles are spherical and homogeneous, the Lorenz–Mie theory can be used to predict the scattering cross-section and asymmetry factor of individual particles [20,24]. By contrast, when particles are touching or are in close proximity, scattering characteristics of the ensemble cannot always be determined by merely adding up

* Corresponding author.
E-mail address: pilon@seas.ucla.edu (L. Pilon).

https://doi.org/10.1016/j.jqsrt.2021.108018
0022-4073/

Nomenclature

C_{abs}	absorption cross-section, nm^2
C_{sca}	scattering cross-section, nm^2
$\bar{d}$	average interparticle distance, nm
f_v	particle volume fraction
g	asymmetry factor
L	size of cubic simulation domain, nm
m	relative refractive index, $m = m_s/n_m = n + ik$
m_s	complex refractive index of the particle, $m_s = n_s + ik_s$
N_s	number of particles in the aggregate
n_{eff}	effective refractive index of the aggregate
n_s	particle refractive index
n_m	refractive index of the surrounding medium
k_s	particle absorption index
Q_{sca}	scattering efficiency factor
R_s	aggregate radius, nm
r_{eff}	effective radius of the aggregate, nm
r_s	particle radius, nm
V_t	total volume occupied by the aggregate, nm^3
x_s	particle size parameter, $x_s = 2\pi r_s/\lambda$
Greek symbols	
χ_s	aggregate size parameter, $\chi_s = 2\pi R_s/\lambda$
λ	wavelength, nm
σ_s	scattering coefficient, nm^{-1}
Supercripts and subscripts	
a	refers to scattering characteristics of aggregates
EEP	refers to the equivalent effective properties approximation
EV	refers to the equivalent volume approximation
eff	refers to effective properties
PC	refers to systems with point-contact particles
SC	refers to systems with surface-contact particles
s	refers to silica

or averaging the contributions of individual particles. This situation is typically referred to as the "dependent scattering regime" [22,23]. For aggregates of non-absorbing monodisperse particles of radius r_s and refractive index n_s surrounded by a medium of refractive index n_m, the transition from dependent to independent scattering regimes for the aggregate's scattering cross-section C^a_{sca} and asymmetry factor g^a depends on (i) the particles size parameter $x_s = 2\pi r_s/\lambda$, (ii) their relative refractive index $m = n_s/n_m$, (iii) the average interparticle distance-to-wavelength ratio $\bar{d}/\lambda$, and (iv) the number N_s of particles in the aggregate [23].

Fig. 2 illustrates the regime map for the scattering cross-section of aggregates plotting the particle size parameter x_s versus the average interparticle distance-to-wavelength ratio $\bar{d}/\lambda$ based on our previous study [23]. The transition from dependent to independent scattering regimes corresponded to a relative difference in the predicted scattering cross-section exceeding 5%. The transition occurs for an average interparticle distance-to-wavelength ratio $\bar{d}/\lambda = 2$ for $x_s \leq 2$ and $\bar{d}/\lambda = 5$ for $x_s > 2$. Note that for the aggregate asymmetry factor, the transition from the dependent to the independent scattering regimes for particles with $x_s > 2$ was also achieved for $\bar{d}/\lambda = 5$. However, for particles with $x_s \leq 2$ the transition was achieved for $\bar{d}/\lambda$ as high as 25 [23]. The effect of the relative refractive index m was shown to be negligible when varied between 0.67 and 2.6 [23]. Fig. 2 also shows the range of x_s and $\bar{d}/\lambda$ relevant to various applications. It indicates that dependent light scattering prevails for various particle systems such as mesoporous materials, atmospheric aerosols, paints, nanofluids, and nanoemulsions.

In the dependent scattering regime, the radiative characteristics of aggregates can be estimated by solving Maxwell's equations using the *T*-matrix [25,26] or the discrete-dipole approximation (DDA) [27] methods, among others. However, these computational approaches can be resource intensive and time-consuming. Thus, simpler, faster, and yet accurate methods would be highly desirable. Previous studies investigating such approximations were limited to non-absorbing aggregates with point-contact particles [22,28] or particle suspensions [29,30] within a narrow range of particle and aggregate sizes. Moreover, overlapping of particles often occurs in actual particle-based systems. For example, sol-gel synthesis of mesoporous coatings and monoliths consists of several consecutive steps including gelation, aging, and drying [31,32]. The aging step involves dissolution of the silica primary particles and reprecipitation of silica in the pore, cracks, and particle neck regions separating two primary particles [31,32]. This process reinforces mechanically the particle network or aggregate and enables the monolith to sustain the subsequent drying. The formation of necks between spherical particles can be approximated as overlapping of adjacent particles, as illustrated in Fig. 1(c) and (d) for nanoparticle-based [14] and molecular precursors [33], respectively.

A large body of work has been published on the radiation characteristics of aggregates and focus on absorbing particles including soot particles and atmospheric dusts. The reader is referred to Refs. [34–36] for an extensive review of the literature. Here, we will limit ourselves to reviewing studies focused on aggregates of non-absorbing particles where diffraction, interferences, dependent and multiple scattering play a central role and are not hindered by absorption. Similarly, the effect of particle overlapping on the radiation characteristics of absorbing aggregates have been investigated in the literature [37–39]. However, to the best of our knowledge, the effect of particle overlapping on the radiation characteristics of non-absorbing aggregates has not been investigated to date.

The present study aims to assess the effects of dependent scattering and particle overlapping on the integral radiation characteristics of fractal aggregates of monodisperse non-absorbing spherical particles with a wide range of particle and aggregate sizes containing up to 30,000 particles. It also aims to identify scattering approximations capable of rapidly predicting these radiation characteristics. To do so, the scattering cross-section and asymmetry factor of aggregates with touching or overlapping non-absorbing particles were computed using the *T*-matrix and DDA methods, respectively. The results were compared with predictions from commonly used scattering approximations modeling aggregates as equivalent homogeneous spheres.

2. Background

2.1. Scattering approximations

There exists numerous approximations predicting the scattering cross-section C^a_{sca} and asymmetry factor g^a of fractal aggregates consisting of monodisperse particles [20,22,28–30,34,40,41]. All approximations require knowing at least (i) the particle size parameter x_s, (ii) the particle relative complex refractive index $m = (n_s + ik_s)/n_m = n + ik$, and (iii) the spatial arrangement of the particles in the aggregate.

For example, the Rayleigh-Debye-Gans (RDG) theory and the anomalous diffraction approximation assume that the phase shift of the wave passing through optically soft spheres satisfies the condition $|m - 1| \ll 1$ [34,40]. On the one hand, the RDG theory predicts the scattering and absorption cross-sections, and the asymmetry factor of aggregates with monodisperse point-contact spheres such that $x_s \ll 1$. Expressions for C^a_{abs}, C^a_{sca}, and g^a not only depend on (i) x_s and (ii) m but also on the aggregate's (iii) frac-

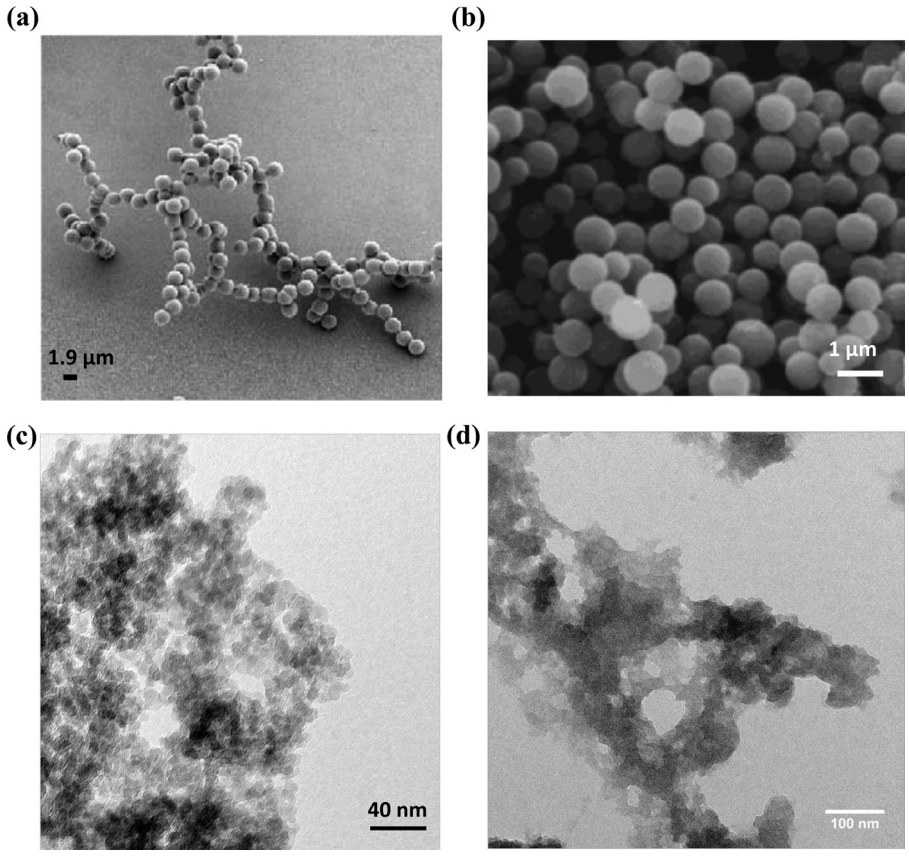

Fig. 1. Scanning electron microscopy images of (a) silica aggregate representative of atmospheric silicate dust [2] and of (b) titania particles used in paints and coatings [9]. Transmission electron microscopy images of (c) nanoparticle-based and (d) ambigel mesoporous silica monoliths.

tal dimension, (vi) radius of gyration, (v) structure factor, and (vi) number of particles N_s [34,40]. On the other hand, the anomalous diffraction approximation considers aggregates consisting of large point-contact particles such that $x_s \gg 1$ [41]. The scattering cross-section C_{sca}^a of the aggregates can be predicted based on (i) x_s, (ii) m, (iii) the chord length of the aggregate, and (iv) the aggregate's projected area [41].

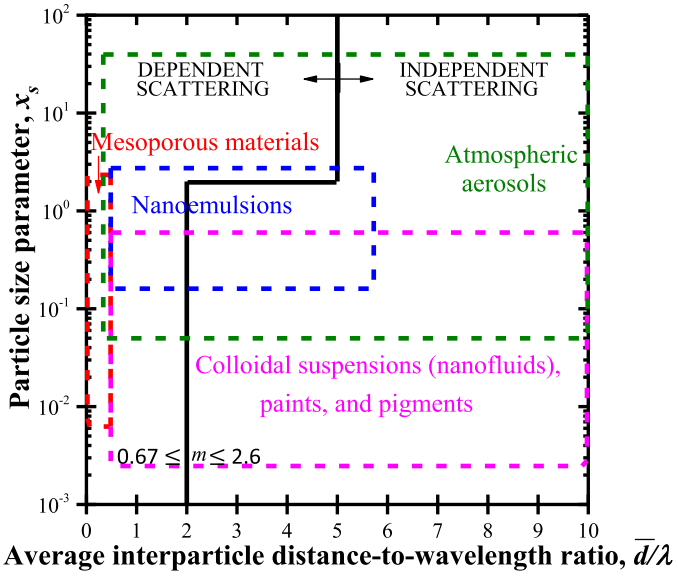

Fig. 2. Scattering regime map for the scattering cross-section plotting zones of typical particle systems with respect to their particle size parameter x_s and average interparticle distance-to-wavelength ratio between constituent particles.

Alternatively, other commonly used approximations model aggregates as equivalent homogeneous spheres [42–44]. These approximations necessitate relatively few structural information about the aggregate and can also be used for aggregates with overlapping (or surface-contact) particles. Two of the most commonly used approximations include the equivalent volume (EV) [20,22] and the equivalent effective properties (EEP) [22,28–30] approximations illustrated in Fig. 3. The EV approximation models the aggregate as an equivalent sphere with the same complex index of refraction as the particles m_s and effective radius r_{eff} such that the volume of the equivalent sphere matches the volume V_s of the aggregate occupied by the particles, i.e.,

$$\frac{4\pi}{3} r_{eff}^3 = V_s = f_v V_t \tag{1}$$

where V_t is the total volume of the aggregate and f_v is the particle volume fraction calculated as the ratio of the volume V_s occupied by the particles to the total volume V_t of the aggregate, i.e., $f_v = V_s/V_t$. For aggregates with monodisperse point-contact particles of radius r_s, V_s can be expressed as $V_s = 4\pi r_s^3 N_s/3$ and Eq. (1) simplifies to $r_{eff} = r_s N_s^{1/3}$.

Moreover, the EEP approximation treats the aggregate as an equivalent sphere of radius R_s encompassing the aggregate such that [28]

$$R_s = (3V_t/4\pi)^{1/3}. \tag{2}$$

Here, the equivalent sphere has an effective refractive index n_{eff} given by some effective medium approximation (EMA) [Fig. 3(c)]. In this study, the 3D Maxwell–Garnett EMA was used to predict

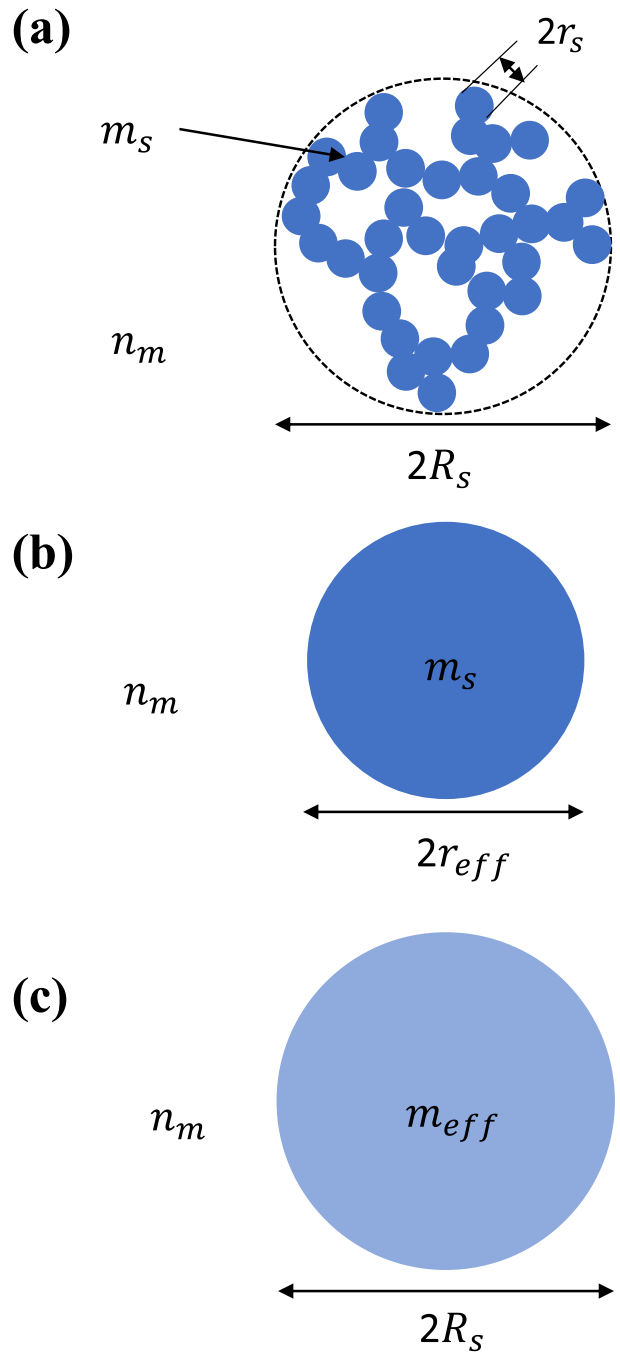

Fig. 3. (a) Particle aggregate and its equivalent representations (b) in the EV approximation and (c) in the EEP approximation.

n_{eff} according to [45]

$$n_{eff}^2 = n_m^2\left[1 - \frac{3f_v(n_m^2 - n_s^2)}{2n_m^2 + n_s^2 + f_v(n_m^2 - n_s^2)}\right]. \quad (3)$$

Finally, in both the EV and EEP approximations, the scattering cross-sections, denoted by C_{sca}^{EV} and C_{sca}^{EEP}, and the asymmetry factors, g^{EV} and g^{EEP}, of their respective equivalent spheres can be predicted using the Lorenz–Mie theory [24].

2.2. Equivalent sphere approximations

Previous studies have investigated the applicability of the EV [20,46] and EEP [28–30,46] approximations for predicting the radiation characteristics of aggregates [28,46] and suspensions [29,30] with monodisperse non-absorbing spherical particles. Drolen and Tien [46] studied the scattering and absorption cross-sections of spherical, cubical, and ellipsoidal clusters and linear chains of touching, spherical, and monodisperse particles with $x_s = 0.00785$, 0.037, and 0.0393 and aggregate size parameter $\chi_s \leq 5$ defined as $\chi_s = 2\pi R_s/\lambda$ where R_s is given by Eq. (2). The number of particles N_s in the aggregates was less than 136 and the particle volume fraction f_v varied from 0.05 to 0.95. The study included aggregates with negligible absorption, i.e., $m = m_s/n_m = 1.5 + i10^{-6}$ and also absorbing aggregates with $m = 2.0 + i0.95$ and $3.5 + i3$. The authors compared the EV and EEP approximations based on the Maxwell–Garnett EMA [Eq. (3)] for both n_{eff} and k_{eff} with predictions from an analytical model based on the solution of Maxwell's equations for spheres in the Rayleigh scattering regime [47,48]. The study showed that predictions by the EV approximation were in good agreement with results from the analytical model for chains with a small number of particles ($N_s < 30$) and for all clusters considered. By contrast, the EEP model was in good agreement with the analytical model for all aggregates investigated.

Lagarrigue et al. [28] investigated the scattering cross-section of non-absorbing and optically hard aggregates with particle size parameter $x_s \leq 0.63$, number of particles $N_s > 13$, and aggregate size parameter $\chi_s \leq 3.14$. The relative refractive index of the monodisperse particles was $m = n_s/n_m = 1.77$ or 1.94. The aggregates were generated in spherical and cubic domains as well as cylindrical or ellipsoidal domains featuring aspect ratios varying from 1/20 to 20. The aggregates' particle volume fraction f_v varied from 0.0605 to 0.605. The generalized multiparticle Mie theory algorithm was used to compute the aggregates scattering cross-section. The authors showed that the applicability of the EEP approximation, based also on the Maxwell–Garnett EMA, depended on the aspect ratio of the aggregate. As the aspect ratio deviated from unity, the EEP approximation differed from the numerical predictions. The study also concluded that the effect of the particle size on the validity of the EEP approximation was negligible. An empirical expression for the scattering cross-section of aggregates was derived by fitting the scattering cross-section of 1792 aggregates with various shapes, sizes, particle size parameters, relative refractive index, and aspect ratios.

Mishchenko et al. [29] used the *T*-matrix method to compute the elements of the normalized scattering matrix of randomly distributed non-touching and non-absorbing spherical particles and compared them to the EEP approximation based on the Maxwell–Garnett EMA. The non-touching particles featured $x_s = 0.3$, 0.5, or 1 and were embedded in a spherical domain with size parameter $\chi_s = 10$. The particle refractive index was $n_s = 1.55$ and that of the surrounding medium was $n_m = 1.33$. The aggregates' particle volume fraction f_v was 0.216 or 0.2 and the number of particles N_s varied from 216 to 8000. The authors showed that suspensions with particles such that $x_s = 0.3$ and 0.5 were within the range of validity of the EEP approximation while those consisting of particles with $x_s = 1$ fell outside. In addition, by comparing results for suspensions with the same particle size parameter $x_s = 0.3$ and different number of particles ($N_s = 500$ and 8000) the authors concluded that N_s should be sufficiently large to ensure the validity of the EEP approximation. However, the authors wrote that "*the threshold value of x_s and N_s can be expected to depend on the refractive indices of the host and the inclusions as well as on the size parameter of the host and should be further analyzed and quantified*".

Mishchenko et al. [30] extended the analysis of Ref. [29] for non-touching particle suspensions to a wider range of particle size parameter x_s and suspension size parameter χ_s representative of air bubbles ($n_s = 1$) and hematite inclusions ($m_s = 3.102 + i0.0925$) in dust material ($n_m = 1.6$). For air bubbles, x_s varied from 0.15 to

1.09, $\chi_s = 4$ or 8, and N_s ranged from 1 to 3,035. For hematite inclusions, x_s varied from 0.1 to 0.5, $\chi_s = 4$ or 8, and N_s ranged from 10 to 10,240. Results were also presented for non-absorbing suspensions of particles with $x_s = 0.3$ or 0.6, $\chi_s = 10$, $N_s = 1000$ and 8000, refractive index n_s varying from 1.4 to 2, and $n_m = 1.32$. The particle volume fraction was $f_v = 0.02$ for air bubbles and hematite particles and $f_v = 0.216$ for other non-absorbing suspensions. The elements of the scattering matrix, the scattering and absorption cross-sections, and the asymmetry factor of the suspensions were computed using the *T*-matrix method and the EEP approximation based on the Maxwell–Garnett EMA for both n_{eff} and k_{eff}. For all cases considered, predictions of the scattering cross-section and asymmetry factor by the EEP approximation fell within 6.5% of those by the *T*-matrix method. However, predictions of the elements of the scattering matrix by the EEP approximation differed significantly from the *T*-matrix calculations for aggregates with $x_s \geq 0.5$. In addition, the difference between predictions of the two methods increased with increasing suspension size parameter and refractive index mismatch between the particles and their surrounding. The authors concluded that a larger refractive index mismatch restricted the range of validity of the EEP approximation to aggregates with smaller particles. This observation suggests that the validity of the EEP approximation depends on the phase shift defined as $2x_s|m-1|$ [22].

Finally, Fig. 4 illustrates the ranges of particle size parameter x_s, aggregate or suspension size parameter χ_s, and phase shift $2x_s|m-1|$ used in the different studies investigating the validity of the EV and EEP approximations for systems consisting of non-absorbing spherical particles [22,28–30]. It indicates that previous studies were limited to relatively small particle size parameter $x_s \leq 1.09$ and aggregate size parameter $\chi_s \leq 10$. Although the refractive index n_s of the particle was sometimes large [28], the particles were relatively small and, therefore, the range of the phase shift $2x_s|m-1|$ explored was limited from ~0 to 1.2. Moreover, to the best of our knowledge, none of the previous studies investigated the effect of particle overlapping on the applicability of the EEP approximation.

The present study aims to evaluate systematically the effects of dependent scattering and particle overlapping and to assess the validity of the EV and EEP approximations in predicting the scattering cross-section C^a_{sca} and the asymmetry factor g^a of aggregates with point-contact and overlapping particles over a significantly larger range of particle and aggregate size parameters than those investigated in previous studies [22,28–30]. In particular, it is interesting to determine if these approximations are also valid when dependent scattering prevails.

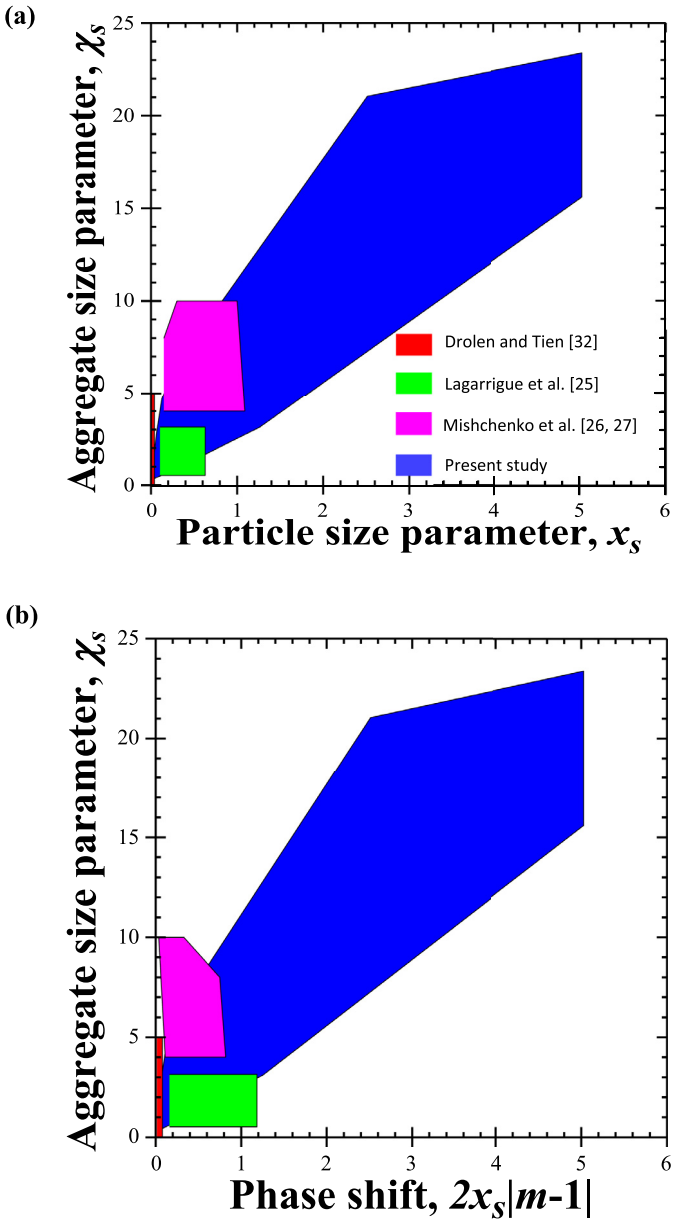

Fig. 4. Comparison of the range of aggregate size parameter χ_s and (a) particle size parameter x_s or (b) optical phase shift $2x_s|m-1|$ in computer-generated aggregates investigated in Refs. [28–30,46] and in the present study.

3. Analysis

3.1. Computer-generated aggregates

The Diffusion-Limited Cluster-Cluster Aggregation (DLCCA) algorithm [49] was used to generate aggregates consisting of N_s spherical monodisperse particles of radius r_s positioned in a three-dimensional cubic domains of side L, as described in Ref. [49]. The spherical simulation domain of radius R_s were cut out of the cubic domains such that every particles falling outside the sphere were removed. For cubic simulation domains, the equivalent sphere radius R_s was defined as the radius of a sphere having the same total volume as the cubic aggregate, i.e., $V_t = L^3$ and was calculated from Eq. (2). Two types of structures were generated namely (1) aggregates with point-contact particles where spherical particles may touch each other at a point but do not overlap and (2) aggregates with surface-contact particles consisting of overlapping spherical particles [49]. The particle radius r_s ranged from 2.5 to 400 nm, R_s varied from 6 nm to 1860 nm, and the wavelength λ was set to 500 nm corresponding to x_s varying from 0.031 to 5.03 and χ_s varying from 0.08 to 23. The number of particles N_s ranged from 5 to 30,000 and the refractive index n_s of the particles was set to $n_s = 1.5$ while the surrounding medium was vacuum, i.e., $n_m = 1$ resulting in $m = 1.5$. Finally, the particle volume fraction f_v of all computer-generated structures was 33 ± 2%. This choice of f_v was arbitrary. However, if the EV or EEP approximations are found to be valid for $f_v = 33 \pm 2\%$, it is reasonable to expect them to be valid for other values of f_v whose effect is accounted for through the equivalent sphere radius r_{eff} [Eq. (1)] or via the effective refraction index n_{eff} [Eq. (3)]. Finally, the overlapping spheres were such that their interparticle distance d - defined as the distance between the center of two adjacent particle's was smaller than the diameter $2r_s$ of a sphere. Then, the overlapping distance can be expressed as $l_0 = d - 2r_s$, and the mean dimensionless overlapping distance as $\bar{l}^* = l_0/2r_s$. For the porosity $1 - f_v \approx 67\%$ considered in the present manuscript, the mean dimensionless overlapping distance was $\bar{l}^* \approx 0.24$ [49].

3.2. Scattering characteristics

The scattering efficiency factor Q^a_{sca} and the asymmetry factor g^a of the computer-generated aggregates with point-contact particles generated numerically was predicted by the multiple sphere *T*-matrix (MSTM) code developed by Mackowski [25] and based on the superposition *T*-matrix method [26]. The input parameters of the MSTM code included (i) the position of the constitutive monodisperse particles, (ii) their size parameter $x_s = 2\pi r_s/\lambda$, and (iii) their relative refractive index m.

To consider the complex geometry of aggregates with surface-contact particles, the discrete-dipole approximation (DDA) algorithm developed by Draine and Flatau [27] was employed. First, N_d dipoles of size Δd were generated inside the N_s particles of the numerically-generated aggregates such that $\sum_{i=1}^{N_d}(\Delta d)^3 = V_s$. The dipoles were such that their size Δd was small compared to the particle radius r_s and wavelength λ to achieve numerically converged results independent of the choice of discretization [50]. Specifically, for all simulations, $\Delta d/r_s \leq 0.2$, $2\pi r_{eff}/\lambda < 7$, $|m-1| \leq 0.5$, and $2\pi r_{eff}/\lambda < 15.51/|m|(N_d/10^6)^{1/3}$. These convergence criteria satisfied or exceeded the criteria given by Draine and Flatau [50]. Finally, note that the DDA simulation code and implementation was successfully validated with the cases of single spheres with size parameters and relative refractive index encountered in the present study. The input parameters of the DDA method predicting Q^a_{sca} and g^a included (i) the position of the N_d dipoles, (ii) the wavelength λ, (iii) the relative refractive index m.

The integral radiative characteristics can be predicted either for aggregates with a given orientation or for randomly oriented aggregates. However, fixed-orientation and orientation-averaged scattering efficiency factors were found to differ by less than 1% and the asymmetry factors by less than 4% for both point-contact and surface-contact aggregates with $x_s \leq 0.13$ (see Table S1 in Supporting Information). This observation was likely due to the fact that small particles with $x_s \leq 0.13$ scatter radiation isotropically resulting in very similar scattering characteristics for different aggregates' orientations. Therefore, simulations for aggregates with point-contact particles such that $x_s \leq 0.13$ and large aggregate size parameter χ_s were performed for a fixed orientation to reduce the computational time. On the other hand, for aggregates with particles such that $x_s > 0.13$, at least 55 aggregate orientations were simulated and the orientation-averaged scattering cross-section and asymmetry factor were reported.

The scattering cross-section C^a_{sca} (in nm^2) of aggregates consisting of N_s monodisperse point-contact or surface-contact particles can be calculated from the radius r_{eff} and the computed efficiency factor Q^a_{sca} according to [25,50]

$$C^a_{sca} = \pi r^2_{eff} Q^a_{sca}. \tag{4}$$

where r_{eff} is the effective radius of the aggregate expressed as $r_{eff} = (3V_s/4\pi)^{1/3}$ [Eq. (1)].

Overall, it took between a couple of minutes and 18 h to perform the different simulations on UCLA Hoffman2 computing cluster. The computational time increased with increasing particle and aggregate size parameters as well as number of particles and relative refractive index. For example, it took 18.03 h to run the simulation for an aggregate with 30,000 monomers such that $x_s = 2.5$, $\chi_s = 23$, and $m_s = 1.5$ using on 8 GB of RAM/core and 16 CPUs.

4. Results and discussion

4.1. Dependent effects in aggregates

Fig. 5 presents the absorption and scattering cross-section ratios $C^a_{abs}/N_sC^M_{abs}$ and $C^a_{sca}/N_sC^M_{sca}$, and asymmetry factor ratio g^a/g^M as functions of χ_s for fractal aggregates with point-contact particles with size parameter $x_s = 0.031$ and 0.63, particle volume fraction $f_v = 33 \pm 2\%$, and relative refractive index $m = n + ik$ such that $n = 1.5$ and $0 \leq k \leq 0.5$. Here, C^M_{abs}, C^M_{sca}, and g^M are the absorption cross-section, scattering cross-section, and asymmetry factor of a single particle of size parameter x_s and relative refractive index m calculated using Lorenz–Mie theory. Ratios $C^a_{abs}/N_sC^M_{abs}$, $C^a_{sca}/N_sC^M_{sca}$, and g^a/g^M equal to unity would indicate that the radiation characteristics of the aggregates represent the cumulative contributions of individual constitutive particles, i.e., the particles absorbed and scattered independently of each other. First, Figs. 5(a)–5(d) establish that dependent effects prevailed in the absorption and scattering of the aggregates considered, as all ratios differed from 1. However, it is interesting to note that the ratio $C^a_{sca}/N_sC^M_{sca}$ was much larger and increased significantly more than $C^a_{abs}/N_sC^M_{abs}$ with increasing aggregate size parameter χ_s. These observations were in agreement with results reported in previous studies [35,51]. Figs. 5(c) and 5(d) also suggest that the increase in the aggregate scattering cross-section ratio $C^a_{sca}/N_sC^M_{sca}$ was larger for aggregates with small particle size parameter x_s. These results indicate that for applications with small absorbing nanoparticles such as those found in concentrated nanofluids for solar energy applications [52–55], the nanoparticles that are likely to aggregate can be assumed to absorb independently (i.e., $C^a_{abs} \approx N_sC^M_{abs}$), but dependent scattering prevails and $C^a_{sca} > N_sC^M_{sca}$.

Fig. 5(b) also shows that the ratio $C^a_{abs}/N_sC^M_{abs}$ decreased with increasing relative absorption index k for any given aggregate with size parameter $\chi_s > 0.6$. For large values of k, C^a_{abs} was even smaller than $N_sC^M_{abs}$. The same findings were presented in Ref. [51] for aggregates consisting of monodisperse particles with $x_s = 1$, $n = 1.0165$, $0 \leq k \leq 0.5$, and $N_s < 1000$. This observation was attributed to the so-called "shielding" or "shading" effect of the aggregate's inner particles by those located at the outer surface of the aggregate and responsible for the increased attenuation of the electromagnetic wave before it reached the inner particles. In addition, Figs. 5(c) and 5(d) indicate that the scattering cross-section ratio $C^a_{sca}/N_sC^M_{sca}$ was not affected by absorption for $\chi_s \leq 0.7$. However, for $\chi_s > 1$, the ratio $C^a_{sca}/N_sC^M_{sca}$ decreased with increasing relative absorption index k for any given value of χ_s [Fig. 5(d)].

Finally, Figs. 5(e) and 5(f) show that dependent scattering effects in aggregates with large size parameter χ_s and small particle size parameter x_s were significant and resulted in $g^a > g^M$. In addition, the effect of the particle relative absorption index k on the asymmetry factor ratio g^a/g^M was negligible despite its strong effect on $C^a_{sca}/N_sC^M_{sca}$ for $x_s = 0.63$. Note that the same conclusions were reached for all three ratios $C^a_{abs}/N_sC^M_{abs}$, $C^a_{sca}/N_sC^M_{sca}$, and g^a/g^M for particle size $x_s = 2.51$, as presented in Figure S1 in Supporting Information.

Overall, Fig. 5 shows that dependent effects were significantly more prominent in the scattering cross-section and asymmetry factor of the aggregates than in their absorption cross-section. Thus, the remainder of this paper focuses on the scattering characteristics C^a_{sca} and g^a of non-absorbing particle aggregates for a wide range of particle x_s and aggregate χ_s size parameters.

4.2. Equivalent models for non-absorbing fractal aggregates

4.2.1. Scattering cross-section C^a_{sca}

Fig. 6(a) plots the scattering cross-section C^a_{sca} predicted by the *T*-matrix method [25,26] as a function of the aggregate size parameter χ_s for fractal aggregates with particle volume fraction $f_v = 33 \pm 2\%$ generated in cubic or spherical domains with point-contact particles of size parameter x_s ranging from 0.031 to 5.03 and relative refractive index $m = 1.5$. Fig. 6(a) also displays the scattering cross-section of the same aggregates predicted by the EV

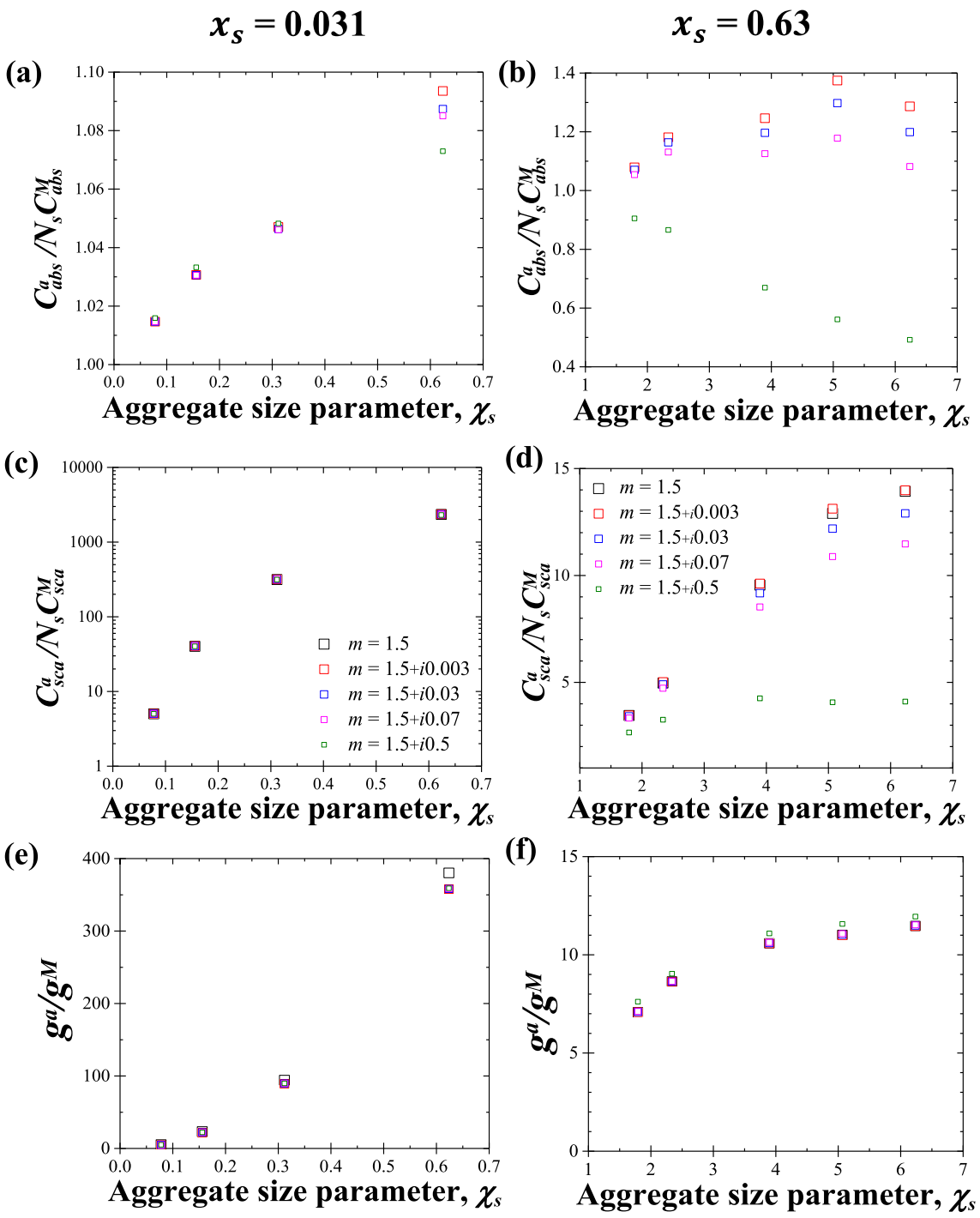

Fig. 5. (a)-(b) Absorption cross-section ratio $C^a_{abs}/N_sC^M_{abs}$, (c)-(d) scattering cross-section ratio $C^a_{sca}/N_sC^M_{sca}$, and (e)-(f) asymmetry factor ratio g^a/N_sg^M as functions of the aggregate size parameter χ_s for aggregates of touching monodisperse particles with size parameter (a, c, e) $x_s = 0.031$ and (b, d, f) $x_s = 0.63$, particle volume fraction $f_v = 33 \pm 2\%$, and relative refractive index m between 1.5 and 1.5+i0.5.

and EEP approximations. First, Fig. 6(a) indicates that the scattering cross-section of aggregates C^a_{sca} increased with increasing aggregate size parameter χ_s for all particle size parameters x_s. Fig. 6(a) also establishes that both the EV and EEP approximations were in good agreement with the T-matrix method predictions of C^a_{sca} for relatively small aggregates with $\chi_s \leq 1$. These observations were consistent with those of Ref. [46] for small aggregates with negligible absorption, i.e., $m = m_s/n_m = 1.5 + i10^{-6}$. However, for $\chi_s > 1$, the scattering cross-section C^a_{sca} of the aggregates differed significantly from that predicted by the EV approximation and was in better agreement with predictions by the EEP approximation. In fact, Figs. S2(a) and S3(a) in Supporting Information present the relative errors in the scattering cross-section between numerical simulations and EEP or EV approximation predictions, respectively, with respect to the aggregate size parameter χ_s for different particle size parameters x_s. First, Fig. S2(a) shows that the relative error $|C^a_{sca} - C^{EEP}_{sca}|/C^a_{sca}$ was less than 15% when $x_s \leq 1$ and $0 \leq \chi_s \leq 23$. However, for $x_s > 1$, $|C^a_{sca} - C^{EEP}_{sca}|/C^a_{sca}$ varied between 0 and 80% for various x_s and χ_s, but no clear and systematic effect of x_s or χ_s could be identified. Moreover, Fig. S3(a) indicates that the relative

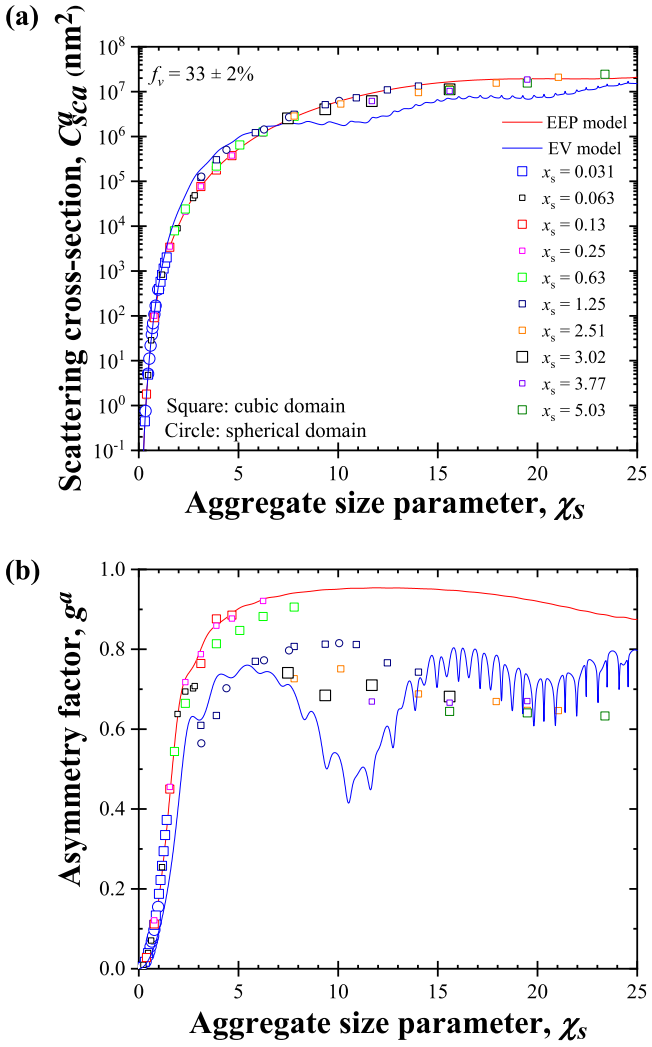

Fig. 6. (a) Scattering cross-section C^a_{sca} and (b) asymmetry factor g^a of point-contact particle aggregates as functions of the aggregate size parameter χ_s for non-absorbing particles with size parameter x_s ranging from 0.031 to 5.03, particle volume fraction $f_v = 33 \pm 2\%$, and relative refractive index $m = 1.5$.

error $|C^a_{sca} - C^{EV}_{sca}|/C^a_{sca}$ overall exceeded 30% in all cases and could reach values as high as 70% even for $x_s \leq 1$.

4.2.2. Asymmetry factor g^a

Fig. 6(b) presents the asymmetry factor g^a as a function of the aggregate size parameter χ_s for non-absorbing aggregates with point-contact particles with x_s varying between 0.031 and 5.03, $m = 1.5$, and particle volume fraction $f_v = 33 \pm 2\%$. It also plots predictions obtained by the EEP and EV approximations. Fig. 6(b) indicates that the aggregates' asymmetry factor g^a depended not only on the aggregate size χ_s but also on the particle size x_s. For given values of χ_s and f_v, aggregates with smaller particles had larger asymmetry factor g^a indicating that they scattered more in the forward direction. Moreover, Fig. 6(b) establishes that the predictions of the EEP approximation for the asymmetry factor of aggregates were also in good agreement with those of the *T*-matrix method for aggregates with small particles such that $x_s < 1$. However, the EV approximation failed to predict g^a accurately for all cases considered. In fact, Figs. S2(b) and S3(b) present the relative error in the asymmetry factor between numerical simulations and EEP or EV approximation predictions, respectively, as a function of the aggregate size parameter χ_s for different values of x_s. Fig. S2(b) indicates that the ratio $|g^a - g^{EEP}|/g^a$ increased from 0 to 50% with increasing particle size parameter x_s and aggregate size parameter χ_s. Moreover, Fig. S2(b) indicates that the relative error $|g^a - g^{EEP}|/g^a$ was less than 15% for aggregates with $x_s \leq 1$ and all size parameter χ_s considered. However, Fig. S3(b) indicates that $|g^a - g^{EV}|/g^a$ was excessively large even for aggregates with small particles $x_s < 1$.

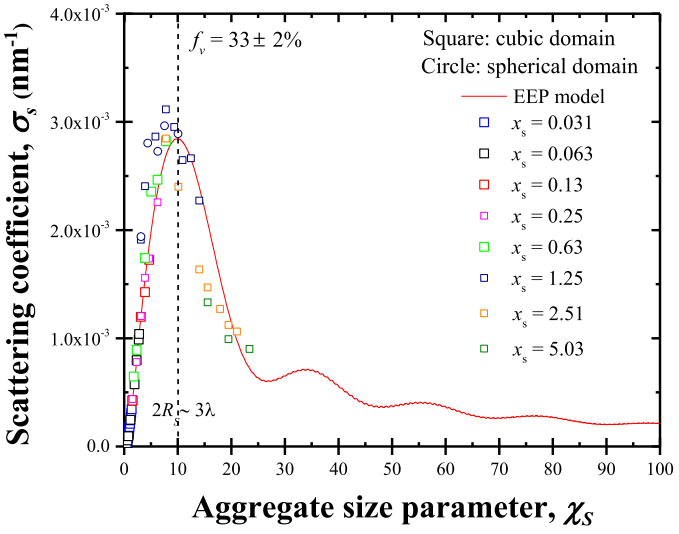

Fig. 7. Scattering coefficient σ_s [Eq. (5)] of point-contact particle aggregates as a function of the aggregate size parameter χ_s for particle size parameter x_s ranging from 0.031 to 5.03, particle volume fraction $f_v = 33 \pm 2\%$, and relative refractive index $m = 1.5$.

Overall, the EEP approximation was found to be valid for all aggregates with particle size parameter $x_s \leq 1$ when the phase shift was small, i.e., $2x_s|m - 1| \leq 1$. In other words, all aggregates with particle size parameter $x_s \leq 1$ could be approximated as homogeneous spheres with the same radius and effective refractive index n_{eff} for the purpose of predicting their cross-section C^a_{sca} and asymmetry factor g^a.

4.2.3. Scattering coefficient σ_s

The scattering coefficient σ_s of the heterogeneous material contained in the aggregate can be defined as [20]

$$\sigma_s = C^a_{sca}/V_t. \tag{5}$$

In case of independent scattering, $C^a_{sca} = N_s C^M_{sca}$ and the scattering coefficient is given by the widely used expression [20]

$$\sigma_s = \frac{N_s}{V_t} C^M_{sca} \tag{6}$$

where N_s/V_t represents the number of particles per unit volume of aggregate. Thus, regardless of the aggregate dimensions, σ_s should be constant, provided independent scattering prevails.

Fig. 7 presents the scattering coefficient σ_s [Eq. (6)] of spherical and cubic aggregates as a function of the size parameter χ_s for particle volume fraction $f_v = 33 \pm 2\%$ (porosity = 67±2%) and point-contact particles featuring x_s between 0.031 and 5.03 and $m = 1.5$. It also plots predictions by the EEP approximation. First, Fig. 7 indicates that the scattering coefficient σ_s increased sharply with increasing size parameter χ_s to reach a maximum at $\chi_s = 10$, corresponding to aggregate diameter $2R_s \approx 3\lambda$. However, as χ_s increased above 10, σ_s decreased sharply in good agreement with predictions by the EEP approximation which featured oscillations for $\chi_s \geq 25$. Moreover, Fig. 7 shows that numerical predictions of σ_s were independent of x_s and of the aggregate shape (cubic or spherical) when $\chi_s \leq 4$. For $\chi_s > 4$, σ_s depended slightly on the particle size x_s and on the aggregate shape. Note that the predictions of σ_s by the *T*-matrix and by the EEP approximation de-

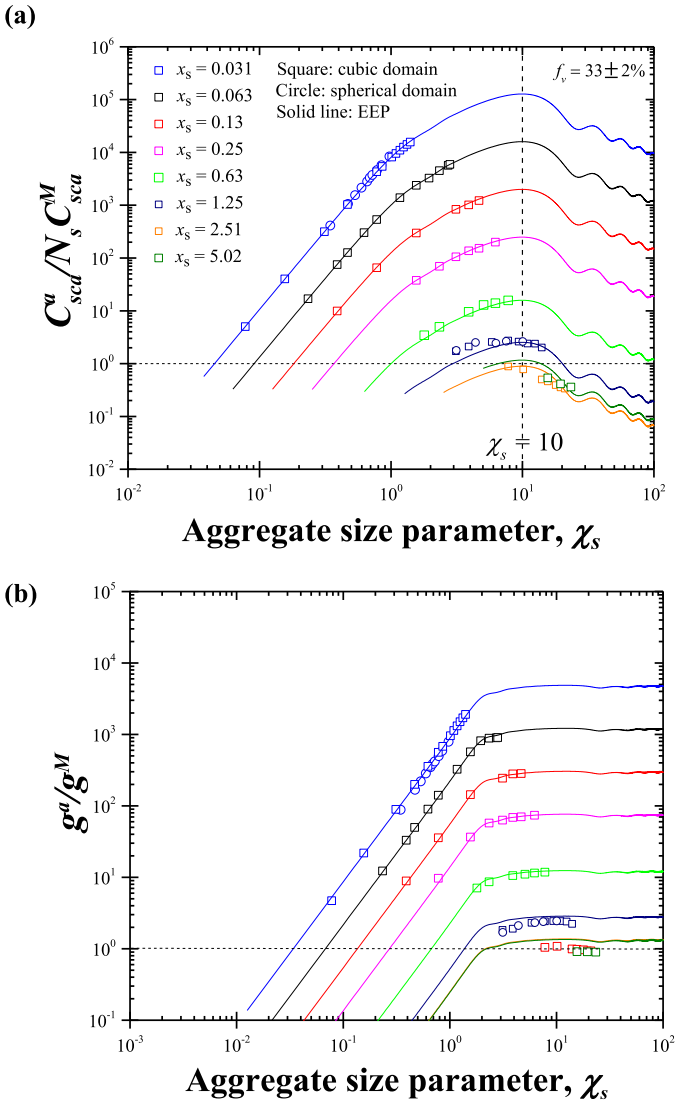

Fig. 8. (a) Scattering cross-section ratio $C^a_{sca}/N_s C^M_{sca}$ and (b) asymmetry factor ratio g^a/g^M of point-contact aggregates of non-absorbing and monodisperse spherical particles as functions of the aggregate size parameter χ_s for particle size parameter x_s ranging from 0.031 to 5.03, particle volume fraction $f_v = 33 \pm 2\%$, and relative refractive index $m = 1.5$.

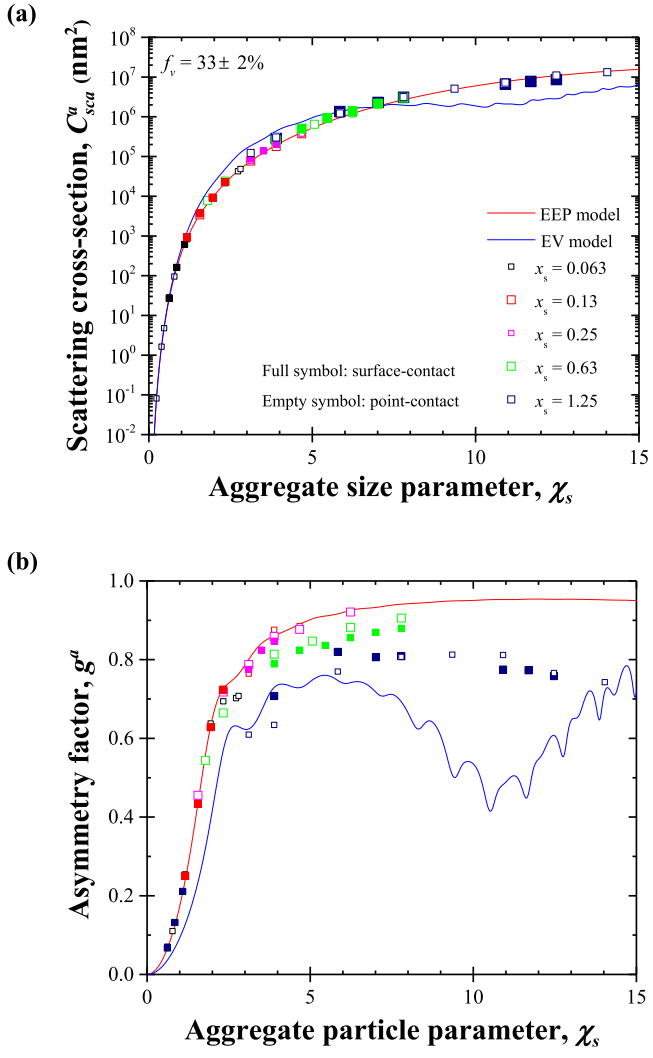

Fig. 9. (a) Scattering cross-section C^a_{sca} and (b) asymmetry factor g^a of point-contact and surface-contact aggregates of non-absorbing and monodisperse spherical particles as functions of the aggregate size parameter χ_s for particle size parameter x_s between 0.063 and 1.25, particle volume fraction $f_v = 33 \pm 2\%$, and $m = 1.5$. Also shown are predictions by the EEP and EV approximations.

creased as χ_s increased and did not converged to a constant value for large values of χ_s (see Figure S4 in Supporting Information). This indicates that predicting the scattering coefficient of mesoporous monoliths, films, or bulk materials from those of aggregates corresponding to a sufficiently large representative elementary volume (REV), as performed in the literature [55,56], is not appropriate. Instead, the scattering and absorption coefficients of monoliths depend on the specific nanoscale architecture (e.g., particle size, porosity, fractal dimension). Thus, they can be retrieved experimentally from the measured transmittance and reflectance by solving the inverse problem [16]. Numerically, determining the scattering and absorption coefficients of monoliths would require solving Maxwell's equations through the entire structure as performed by Mackowski and Mishchenko [57] for a cylindrical volume consisting of nonoverlapping spheres and with a radius ranging from $30r_s$ and $40r_s$, a thickness $L \leq 10r_s$, and $f_v = 50\%$.

4.2.4. Dependent scattering effects

Fig. 8 plots the (a) scattering cross-section ratio $C^a_{sca}/N_s C^M_{sca}$ and (b) asymmetry factor ratio g^a/g^M as functions of the aggregate size parameter χ_s for the same range of parameters considered previously including $0.031 \leq x_s \leq 5.03$ and $m = 1.5$. First, Fig. 8 indicates that C^a_{sca} deviated from $N_s C^M_{sca}$ more strongly for small values of x_s such that $x_s < 0.13$. Indeed, smaller particles scatter radiation isotropically resulting in increased multiple scattering within the aggregates. This observation was consistent with the conclusions of our previous study [23] for aggregates and suspensions with $2 \leq N_s \leq 8$. Moreover, Fig. 8 indicates that dependent scattering effects resulted in $C^a_{sca}/N_s C^M_{sca} > 1$ and $g^a/g^M > 1$ for $2x_s|m-1| < 2.5$ and in $C^a_{sca}/N_s C^M_{sca} < 1$ and $g^a/g^M \sim 1$ for $2x_s|m-1| \geq 2.5$. Interestingly, Fig. 8(a) suggests that $C^a_{sca}/N_s C^M_{sca}$ reached its maximum when $\chi_s \simeq 10$ and then decreased with decreasing χ_s, as observed with σ_s (Fig. 7). On the other hand, the asymmetry factor ratio g^a/g^M increased with increasing χ_s and then reached a plateau for $\chi_s > 2$. Finally, Fig. 8 establishes that the EEP approximation predicted the scattering cross-section and asymmetry factor with a relative error of 15% for aggregates with $2x_s|m-1| \leq 1$ even when dependent scattering prevailed.

Overall, the applicability of the EEP approximation indicates that there are two asymptotic regimes for systems consisting of small particles such that $2x_s|m-1| \leq 1$. When the particle sus-

pension is dilute and the particles are far apart from one another, independent scattering prevails and the scattering coefficient and asymmetry factor of the system are determined by the sum of the contribution of each individual particles [20]. On the other hand, when the particles are touching and forming an aggregate, the scattering characteristics are determined by the size of the aggregate and its effective refractive index such that the EEP approximation is valid while dependent scattering prevails. Furthermore, note that the EEP approximation is still a "phenomenological model" [29,30,58] that has not been derived from Maxwell's equations [30,58]. However, the validity of the EEP approximation when dependent scattering prevails suggests its "*existence must follow from the fundamental laws of classical electromagnetics under quite specific assumptions*" [30].

4.3. Effect of particle overlapping

Fig. 9 plots (a) the scattering cross-section C^a_{sca} and (b) asymmetry factor g^a of aggregates as functions of χ_s for cubic aggregates with $f_v = 33 \pm 2\%$ and with either point-contact or surface-contact (i.e., overlapping) particles with x_s ranging from 0.063 and 1.25. It also shows predictions by the EEP and EV approximations. First, Fig. 9 indicates that overlapping between particles did not strongly affect the scattering characteristics of the aggregates. Indeed, the scattering cross-section C^a_{sca} and asymmetry factor g^a of aggregates with surface-contact particles fell respectively within 15% and 10% of those of the equivalent aggregates with point-contact particles with the same aggregate size χ_s, particle size parameter x_s, and particle volume fraction f_v (see Table S2 in Supporting Information). Similar results were obtained for different values of particle volume fraction f_v associated with different particle overlapping distance $\bar{l}^*$. Figure S5 of Supplementary Materials compares the scattering cross-section of aggregates as a function of particle volume fraction f_v or porosity ϕ for either point-contact or overlapping particles. Simulations were performed using cubic domains with $L = 100$, 200, and 400 nm for particle radius $r_s = 2.5$, 5, and 10 nm, respectively. The wavelength of light was taken as $\lambda = 500$ nm. Predictions by the Rayleigh-Debye-Gans approximation were also plotted to guide the eyes. Predictions for surface-contact structures were nearly identical to those for point-contact structures for any given particle volume fraction. In other words, the effect of particle radius and volume fraction dominated over that of particle overlapping. These observations suggest that the scattering cross-section and asymmetry factor of non-absorbing aggregates were mainly dependent on (i) the aggregate size parameter χ_s, the particles (ii) size parameter x_s, volume fraction f_v, and (iii) the relative refractive index m of the particles. Finally, here also the EEP approximation was valid for aggregates with overlapping particles when $2x_s|m-1| \leq 1$.

5. Conclusions

This study investigated the scattering cross-section and asymmetry factor of aggregates consisting of touching or overlapping non-absorbing spherical particles for a wide range of particle size parameter $0.03 \leq x_s \leq 5$ and aggregate size parameter $0 \leq \chi_s \leq 23$. The aggregates integral radiation characteristics of fractal aggregates with touching or overlapping particles were computed using the *T*-matrix method or the discrete-dipole approximation, respectively. The validity of the EV and EEP approximations treating the heterogeneous aggregates as homogeneous spheres with equivalent radius or refractive index were also evaluated. The results established that dependent effects were more significant in the scattering cross-section and asymmetry factor than in the absorption cross-sections and increased with decreasing particle size parameter. Furthermore, the results indicate that the scattering coefficient of aggregates of any size cannot be used to model light transfer through silica nanoporous monoliths or aerogels. This study also showed that particle overlapping had no significant effect on the scattering cross-section and asymmetry factor of non-absorbing aggregates for the range of size parameters considered. Finally, the study demonstrated that the EEP approximation could predict the scattering cross-section and asymmetry factor of non-absorbing aggregates consisting of small particles such that the phase shift $2x_s|m-1| \leq 1$. Interestingly, the range of validity of the EEP approximation coincided with the dependent scattering regime.

Declaration of Competing Interest

Authors declare that they have no conflict of interest.

CRediT authorship contribution statement

Tiphaine Galy: Conceptualization, Methodology, Formal analysis, Data curation, Visualization, Writing – original draft. **Laurent Pilon:** Conceptualization, Methodology, Formal analysis, Project administration, Supervision, Writing – review & editing.

Acknowledgments

This material is based upon work supported in part by the Advanced Research Projects Agency-Energy (ARPA-E) and its Single-Pane Highly Insulating Efficient Lucid Designs (SHIELD) program (ARPA-E Award no. DE-AR0000738) and the National Science Foundation (NSF) under Grant no. DGE-1735325. This work also used computational and storage services associated with the Hoffman2 Shared Cluster provided by UCLA Institute for Digital Research and Education's Research Technology Group. Tiphaine Galy is grateful to the UCLA Mechanical and Aerospace Engineering Department for financial support through a graduate research fellowship. The authors would also like to thank Dr. Michal Marszewski, Patricia E. McNeil, Maggie Fox, and Sophia C. King for the TEM images of nanoparticle-based and ambigel mesoporous silica monoliths [Figs. 1(c) and 1(d)].

Supplementary material

Fixed-orientation and orientation-averaged scattering cross-section and asymmetry factor of aggregates with point-contact particles (Table S1). Scattering cross-section and asymmetry factor of aggregates with point-contact and surface-contact particles (Table S2). Absorption cross-section ratio, scattering cross-section ratio, and asymmetry factor of aggregates with $x_s = 2.51$, $m = 1.5$, and $f_v = 33 \pm 2\%$ as functions of χ_s (Fig. S1). Relative errors between numerical simulations and EEP predictions for the scattering cross-section and asymmetry factor of aggregates (Fig. S2). Relative errors between numerical simulations and EV predictions for the scattering cross-section and asymmetry factor of aggregates (Fig. S3). Scattering coefficient predicted by the EEP approximation as a function of χ_s (Fig. S4).

Supplementary material associated with this article can be found, in the online version, at doi:10.1016/j.jqsrt.2021.108018

References

[1] Faith W. The atmospheric dust problem. J Air Pollut Control Assoc 1964;14(1):27–9. doi:10.1080/00022470.1964.10468236.
[2] Wurm G, Relke H, Dorschner J, Krauß O. Light scattering experiments with micron-sized dust aggregates: results on ensembles of SiO_2 monospheres and of irregularly shaped graphite particles. J Quant Spectrosc Radiat Transf 2004;89(4):371–84. doi:10.1016/j.jqsrt.2004.05.036.
[3] Kok J, Ridley D, Zhou Q, Miller R, Zhao C, Heald C, Ward D, Albani S, Haustein K. Smaller desert dust cooling effect estimated from analysis of dust size and abundance. Nat Geosci 2017;10(4):274–8. doi:10.1038/NGEO2912.

[4] Mishchenko M, Cairns B, Hansen J, Travis L, Burg R, Kaufman Y, Martins J, Shettle E. Monitoring of aerosol forcing of climate from space: analysis of measurement requirements. J Quant Spectrosc Radiat Transf 2004;88(3):149–61. doi:10.1016/j.jqsrt.2004.03.030.

[5] Auger J-C, Barrera R, Stout B. Scattering efficiency of clusters composed by aggregated spheres. J Quant Spectrosc Radiat Transf 2003;79:521–31. doi:10.1016/S0022-4073(02)00305-9.

[6] Paz Y, Luo Z, Rabenberg L, Heller A. Photooxidative self-cleaning transparent titanium dioxide films on glass. J Mater Res 1995;10(11):2842–8. doi:10.1557/JMR.1995.2842.

[7] Gohin M, Allain E, Chemin N, Maurin I, Gacoin T, Boilot J-P. Sol–gel nanoparticulate mesoporous films with enhanced self-cleaning properties. J Photochem Photobiol A 2010;216(2–3):142–8. doi:10.1016/j.jphotochem.2010.06.029.

[8] Faure B, Salazar-Alvarez G, Ahniyaz A, Villaluenga I, Berriozabal G, De Miguel Y, Bergström L. Dispersion and surface functionalization of oxide nanoparticles for transparent photocatalytic and UV-protecting coatings and sunscreens. Sci Technol Adv Mater 2013;14(2):023001. doi:10.1088/1468-6996/14/2/023001/meta.

[9] Park H, Kim D, Kim C. Effect of solvent on Titania particle formation and morphology in thermal hydrolysis of $TiCl_4$. J Am Ceram Soc 1997;80(3):743–9. doi:10.1111/j.1151-2916.1997.tb02891.x.

[10] Nordgaard A, Beckman W. Modelling of flat-plate collectors based on monolithic silica aerogel. Solar Energy 1992;49(5):387–402. doi:10.1016/0038-092X(92)90111-M.

[11] McEnaney K, Weinstein L, Kraemer D, Ghasemi H, Chen G. Aerogel-based solar thermal receivers. Nano Energy 2017;40:180–6.

[12] Strobach E, Bhatia B, Yang S, Zhao L, Wang E. High temperature annealing for structural optimization of silica aerogels in solar thermal applications. J Non-Cryst Solids 2017;462:72–7.

[13] Baetens R, Jelle BP, Gustavsen A. Aerogel insulation for building applications: a state-of-the-art review. Energy Build 2011;43(4):761–9. doi:10.1016/j.enbuild.2010.12.012.

[14] Marszewski M, King S, Yan Y, Galy T, Li M, Dashti A, Butts D, Kang J, McNeil P, Lan E, Dunn B, Hu Y, Tolbert S, Pilon L. Thick transparent nanoparticle-based mesoporous silica monolithic slabs for thermally insulating window materials. ACS Appl Nano Mater 2019;2(7):4547–55.

[15] Jensen K, Schultz J, Kristiansen F. Development of windows based on highly insulating aerogel glazings. J Non-Cryst Solids 2004;350:351–7.

[16] Zhao L, Yang S, Bhatia B, Strobach E, Wang E. Modeling silica aerogel optical performance by determining its radiative properties. AIP Adv 2016;6(2):1–8. doi:10.1063/1.4943215.

[17] Ganesan K, Lipinski W. Experimental determination of spectral transmittance of porous cerium dioxide in the range 900–1700 nm. ASME J Heat Transf 2011;133(10):104501. doi:10.1115/1.4003970.

[18] Ramezan pour B, Mackowski DW. Radiative transfer equation and direct simulation prediction of reflection and absorption by particle deposits. J Quant Spectrosc Radiat Transf 2017;189:361–8. doi:10.1016/j.jqsrt.2016.11.028.

[19] Zhao L, Strobach E, Bhatia B, Yang S, Leroy A, Zhang L, Wang EN. Theoretical and experimental investigation of haze in transparent aerogels. Optics Express 2019;27(4):A39–50. doi:10.1364/OE.27.000A39.

[20] Modest M. Radiative heat transfer. Academic Press, San Diego, CA, USA; 2013.

[21] Mishchenko M. “Independent” and “dependent” scattering by particles in a multi-particle group. OSA Contin 2018;1(1):243–60. doi:10.1364/OSAC.1.000243.

[22] Tien C-L, Drolen B. Thermal radiation in particulate media with dependent and independent scattering. Annu Rev Heat Transf 1987;1(1):1–32. doi:10.1615/AnnualRevHeatTransfer.v1.30.

[23] Galy T, Huang D, Pilon L. Revisiting independent versus dependent scattering regimes in suspensions or aggregates of spherical particles. J Quant Spectrosc Radiat Transf 2020;246:106924. doi:10.1016/j.jqsrt.2020.106924.

[24] Bohren C, Huffman D. Absorption and scattering of light by small particles. John Wiley & Sons, New York, NY, USA; 1983.

[25] Mackowski D, Mishchenko M. A multiple sphere T-matrix Fortran code for use on parallel computer clusters. J Quant Spectrosc Radiat Transf 2011;112(13):2182–92.

[26] Mackowski D. A general superposition solution for electromagnetic scattering by multiple spherical domains of optically active media. J Quant Spectrosc Radiat Transf 2014;133:264–70.

[27] Draine B, Flatau P. Discrete-dipole approximation for scattering calculations. J Opt Soc Am A 1994;11(4):1491–9.

[28] Lagarrigue M, Jacquier S, Debayle J, Pinoli J-C, Gruy F. Approximation for the light scattering cross-section of optically hard aggregates. J Quant Spectrosc Radiat Transf 2012;113(9):704–14. doi:10.1016/j.jqsrt.2012.02.019.

[29] Mishchenko M, Dlugach Z, Zakharova N. Direct demonstration of the concept of unrestricted effective-medium approximation. Opt Lett 2014;39(13):3935–8. doi:10.1364/OL.39.003935.

[30] Mishchenko M, Dlugach J, Liu L. Applicability of the effective-medium approximation to heterogeneous aerosol particles. J Quant Spectrosc Radiat Transf 2016;178:284–94. doi:10.1016/j.jqsrt.2015.12.028.

[31] Montes S, Maleki H. Chapter 12: aerogels and their applications. In: Thomas S, Sunny AT, Velayudhan P, editors. Colloidal metal oxide nanoparticles. Elsevier; 2020. p. 337–99.

[32] Brinker C, Scherer G. Sol-gel science: the physics and chemistry of sol-gel processing. Elsevier Science; 2013.

[33] Butts D, McNeil P, Marszewski M, Lan E, Galy T, Li M, Kang J, Ashby D, King S, Tolbert S, Hu Y, Pilon L, Dunn B. Engineering mesoporous silica for superior optical and thermal properties. MRS Energy Sustain 2020;7:E39. doi:10.1557/mre.2020.40.

[34] Sorensen C. Light scattering by fractal aggregates: a review. Aerosol Sci Technol 2001;35(2):648–87. doi:10.1080/02786820117868.

[35] Liu L, Mishchenko M. Effects of aggregation on scattering and radiative properties of soot aerosols. J Geophys Res 2005;110:D11211. doi:10.1029/2004JD005649.

[36] Wu Y, Gu X, Cheng T, Xie D, Yu T, Chen H, Guo J. The single scattering properties of the aerosol particles as aggregated spheres. J Quant Spectrosc Radiat Transf 2012;113(12):1454–66. doi:10.1016/j.jqsrt.2012.03.015.

[37] Skorupski K, Hellmers J, Feng W, Mroczka J, Wriedt T, Mädler L. Influence of sintering necks on the spectral behaviour of ITO clusters using the discrete dipole approximation. J Quant Spectrosc Radiat Transf 2015;159:11–18.

[38] Yon J, Bescond A, Liu F. On the radiative properties of soot aggregates part 1: necking and overlapping. J Quant Spectrosc Radiat Transf 2015;162:197–206.

[39] Doner N, Liu F. Impact of morphology on the radiative properties of fractal soot aggregates. J Quant Spectrosc Radiat Transf 2017;187:10–19.

[40] Farias T, Carvalho M, Köylü Ü, Faeth G. Computational evaluation of approximate Rayleigh–Debye–Gans/fractal-aggregate theory for the absorption and scattering properties of soot. ASME J Heat Transf 1995;117(1):152–9. doi:10.1115/1.2822296.

[41] Jacquier S, Gruy F. Anomalous diffraction approximation for light scattering cross section: case of ordered clusters of non-absorbent spheres. J Quant Spectrosc Radiat Transf 2008;109(5):789–810. doi:10.1016/j.jqsrt.2007.09.003.

[42] Chýlek P, Videen G. Scattering by a composite sphere and effective medium approximations. Opt Commun 1998;146(1):15–20.

[43] Kahnert M, Nousiainen T, Lindqvist H, Ebert M. Optical properties of light absorbing carbon aggregates mixed with sulfate: assessment of different model geometries for climate forcing calculations. Opt Express 2012;20(9):10042–58.

[44] Kahnert M. Modelling radiometric properties of inhomogeneous mineral dust particles: applicability and limitations of effective medium theories. J Quant Spectrosc Radiat Transf 2015;152:16–27.

[45] Sihvola A. Electromagnetic mixing formulas and applications, vol 47. The Institution of Electrical Engineers, London, UK; 1999.

[46] Drolen B, Tien C-L. Absorption and scattering of agglomerated soot particulate. J Quant Spectrosc Radiat Transf 1987;37(5):433–48. doi:10.1016/S0022-4073(87)90090-2.

[47] Jones A. Electromagnetic wave scattering by assemblies of particles in the Rayleigh approximation. Proc R Soc Lond. A 1979;366(1724):111–27. doi:10.1098/rspa.1979.0042.

[48] Jones A. Scattering efficiency factors for agglomerates for small spheres. J Phys D 1979;12(10):1661–72. doi:10.1088/0022-3727/12/10/007.

[49] Galy T, Mu D, Marszewski M, Pilon L. Computer-generated mesoporous materials and associated structural characterization. Comput Mater Sci 2019;157:156–67. doi:10.1016/j.commatsci.2018.10.035.

[50] B. Draine, P. Flatau, User guide for the discrete-dipole approximation code DDSCAT 7.3, arXiv preprint arXiv:1305.6497(2013).

[51] Kandilian R, Heng R-L, Pilon L. Absorption and scattering by fractal aggregates and by their equivalent coated spheres. J Quant Spectrosc Radiat Transf 2015;151:310–26. doi:10.1016/j.jqsrt.2014.10.018.

[52] Kameya Y, Hanamura K. Enhancement of solar radiation absorption using nanoparticle suspension. Solar Energy 2011;85(2):299–307. doi:10.1016/j.solener.2010.11.021.

[53] Taylor R, Phelan P, Otanicar T, Adrian R, Prasher R. Nanofluid optical property characterization: towards efficient direct absorption solar collectors. Nanoscale Res Lett 2011;6(1):2–11. doi:10.1186/1556-276X-6-225.

[54] Saidur R, Meng T, Said Z, Hasanuzzaman M, Kamyar A. Evaluation of the effect of nanofluid-based absorbers on direct solar collector. Int J Heat Mass Transf 2012;55(21-22):5899–907. doi:10.1016/j.ijheatmasstransfer.2012.05.087.

[55] Du M, Tang G. Optical property of nanofluids with particle agglomeration. Solar Energy 2015;122:864–72. doi:10.1016/j.solener.2015.10.009.

[56] Schneiderheinze D, Hillman T, Sampson D. Modified discrete particle model of optical scattering in skin tissue accounting for multiparticle scattering. Opt Express 2007;15(23):15002–10. doi:10.1364/OE.15.015002.

[57] Mackowski D, Mishchenko M. Direct simulation of extinction in a slab of spherical particles. J Quant Spectrosc Radiat Transf 2013;123:103–12. doi:10.1016/j.jqsrt.2013.02.008.

[58] Mishchenko M, Dlugach J, Yurkin M, Bi L, Cairns B, Liu L, Panetta R, Travis L, Yang P, Zakharova N. First-principles modeling of electromagnetic scattering by discrete and discretely heterogeneous random media. Phys Rep 2016;632:1–75. doi:10.1016/j.physrep.2016.04.002.